

Modeling Boundary Layer Ingestion Using a Coupled Aeropropulsive Analysis

Justin Gray^{*}, Charles A. Mader[†], Gaetan K.W. Kenway[‡], Joaquim R. R. A. Martins[§]

The single-aisle turboelectric aircraft with an aft boundary layer propulsor aircraft concept is estimated to reduce fuel burn by 12% through a turbo-electric propulsion system with an electrically driven boundary layer ingestion propulsor mounted on the fuselage tail cone. This motivates a more detailed study of the boundary layer ingestion propulsor design, which requires considering the fully coupled airframe propulsion integration problem. However, boundary layer ingestion studies so far have accounted only for the aerodynamic effects on the propulsion system or vice-versa, but have not considered the two-way coupling. This work presents a new approach for building fully coupled propulsive-aerodynamic models of boundary layer ingestion propulsion systems. A one-dimensional thermodynamic cycle analysis is coupled to a RANS simulation. We use this aero-propulsive model to assess how the propulsor design affects the overall performance for a simplified model of the STARC-ABL. The results indicate that both propulsion and aerodynamic effects contribute equally toward the overall performance, and that the fully coupled model yields substantially different results compared to the uncoupled model. Although boundary layer ingestion offers substantial fuel burn savings, it introduces propulsion-dependent aerodynamic effects that need to be accounted for.

Nomenclature

$()^{\text{FE}}$	quantity computed at the fan exit boundary
$()^{\text{FF}}$	quantity computed at the fan-face boundary
$()_{\infty}$	free stream quantity
δ	boundary layer height
\dot{m}	mass flow rate
η_a	adiabatic efficiency
η_p	propulsive efficiency
\mathcal{R}	residual function
ρ	air density
A_{ref}	reference wing area
$C_{F_{\text{fuse}}}$	force coefficient for forces generated by the fuselage
$C_{F_{\text{prop}}}$	force coefficient for forces generated by the propulsor
C_{F_x}	net force coefficient
d_{nac}	nacelle outer diameter
F_{fuse}	force integrated over the fuselage
F_{prop}	force integrated over the propulsor
F_x	net force integrated over the body
l_{ref}	reference length

^{*}Aerospace Engineer NASA Glenn Research Center, PSA Branch, 21000 Brookpark Rd., MS 5-11; Doctoral Candidate Department of Aerospace Engineering, University of Michigan; AIAA Member

[†]Research Investigator, Department of Aerospace Engineering, AIAA Senior Member

[‡]Aerospace Engineer, Science and Technology Corporation; AIAA Senior Member

[§]Professor, Department of Aerospace Engineering; AIAA Associate Fellow

p_s	static pressure
p_t	total pressure
T_t	total temperature
V	air speed
FPR	fan pressure ratio

I. Introduction

Although boundary layer ingestion (BLI), or wake ingestion, has been well studied for marine applications since the 1960s [1, 2, 3] it has not yet seen widespread adoption in aircraft applications. However, recent studies have considered several new BLI-based aircraft configurations that could offer a reduction in aircraft fuel burn between 5% and 12% [4, 5, 6]. This dramatic fuel burn reduction is achieved via tight integration of the propulsion system and airframe aerodynamics, but realizing such large performance gains requires modifying the aircraft design process to account for the interactions between the two systems. The traditional approach to airframe and the propulsion system design is to design them separately, and then size the engine using simple thrust scaling. This works well when the propulsion system is placed in freestream air, away from the aerodynamic influence of the airframe. In this case, it is reasonable to assume that small changes to either system do not affect the other.

This assumption is no longer valid for BLI configurations because changes to the airframe shape directly affect the flow coming into the propulsor, and conversely, changes in the propulsor design directly affect the flow over the airframe. In 1947, the first theoretical study of BLI noted that BLI would introduce a significant dependence between aircraft drag and engine airflow [7]. Decades later, Smith [8] quantified this interaction from the propulsion system perspective, by relating the propulsive efficiency to a set of non-dimensional viscous wake parameters. He found that BLI can increase the overall propulsive efficiency above one, which would be considered a nonphysical result in a stand-alone propulsion system. These efforts highlight the main challenge of modeling aircraft performance in the presence of BLI: The aerodynamic models must be a function of propulsion mass flow, and the propulsion models must be a function of the boundary layer profile. Drela [9] proposed a control volume approach to the aerodynamic bookkeeping as a way to sidestep this issue. Another approach for a more unified bookkeeping approach is to use the exergy concept to quantify the overall efficiency [10, 11].

Despite addressing the thrust and drag accounting problem, the efforts described above did not model the aeropropulsive coupling that is required to capture the multidisciplinary interactions that impact the overall aircraft performance. A number of studies considered the effects of BLI using techniques that capture only part of the coupling. Hardin et al. [12] found up to 10% fuel burn reduction for a BLI propulsion system with a traditional turbofan propulsion modeled using a 1D propulsion model, but their work used a fixed boundary layer profile computed on a clean aircraft a priori with a Reynolds-averaged Navier–Stokes (RANS) solver. Kim and Liou [13, 14] performed a series of aerodynamic shape optimizations on a RANS model of NASA’s hybrid-wing body (HWB) with BLI propulsion systems using powered boundary conditions, but did not consider propulsor design variables and used a linear surrogate for the propulsion model. Blumenthal et al. [15] analyzed a tail cone thruster using an actuator disk approach to add the propulsor into a RANS simulation of the Common Research Model configurations and found that BLI offered a 14% reduction in propulsor power compared to a podded configuration. However, their work kept the diameter of and pressure change across the actuator disk constant, which amounts to a fixed propulsor design. There have also been a number of propulsion-centric studies on BLI propulsion systems, but these did not consider the changes to the flow field due to the presence of the engine [5, 16, 17, 4]. All these studies are motivated by the BLI benefits arising from interdisciplinary interactions, but they make assumptions to partially decouple the analyses to make the modeling easier.

Fully coupling the propulsion and aerodynamic analyses for design optimization presents several challenges due to the cost of the analyses, the implementation of the coupling, and the large number of design variables. These challenges have prevented prior work on propulsion-airframe integration from considering the fully coupled system using models with sufficient fidelity. In this work, we tackle some of these challenges and develop the coupled analysis required for BLI design studies.

The first task towards developing a coupled analysis is to select the propulsion and aerodynamic models that capture the relevant physics. The propulsion system performance can be modeled adequately using an inexpensive one-dimensional (1D) thermodynamic model that represents bulk fluid properties with scalar values [18, 19, 20]. There are two main approaches to modeling viscous aerodynamics over three-dimensional (3D) geometries. One approach is the integral boundary layer (IBL) method, which couples an inviscid flow solver to an approximate boundary layer

solver.[21, 22, 23]. Alternatively, we can use a fully viscous analysis, such as RANS computational fluid dynamics (CFD). For our work, we choose RANS to ensure the general applicability to complex 3D geometries that include intersecting surfaces, and highly 3D flows that might include vortices, and boundary layers that are not fully ingested. Although the geometry considered in the present paper is not that complex, we plan to handle more complex cases in the future.

Aerodynamic performance is highly sensitive to shape changes, and thus a parametrization with a large number of shape design variables is required [24]. RANS-based optimization with respect to large numbers of design variables has been made tractable by using gradient-based numerical optimization in conjunction with the adjoint method, which provides an efficient way to compute the required gradients [25, 26, 24, 27].

Thus, we propose to couple a 1D thermodynamic model of the propulsor to a RANS model of the airframe and propulsor geometry to perform BLI studies. To achieve this, we need to develop a coupling method to exchange the data between the two models and to converge the coupled solution. To leverage the efficiency of gradient-based optimization, we also plan to develop a coupled-adjoint approach to compute the derivatives of the coupled system. The coupled adjoint approach, originally developed by Martins et al. [28, 29], has been well established for aerostructural applications [30, 31, 32], but has not yet been extended to aero-propulsive applications.

The ultimate goal of this research is to develop a fully coupled aero-propulsive multidisciplinary design optimization (MDO) framework that can be used to study NASA's STARC-ABL configuration and other airframe-propulsion integration problems. However, in this paper, we focus on the development of the coupled model, and on the assessment of the coupled effects on a simplified geometry of the STARC-ABL configuration. We leverage NASA's OpenMDAO framework to perform the data exchanges and to solve the coupled system [33]. We then use the coupled model to quantify the effects of fan pressure ratio (FPR) on the overall performance of the aero-propulsive system. Our results show that with BLI, there is a strong and mutually beneficial interaction between the airframe aerodynamics and the propulsor. Furthermore, we show that an uncoupled analysis method misses key multidisciplinary interactions, such as propulsion-dependent lift, drag, and pitching moment.

II. The STARC-ABL Aircraft Configuration

In 2016, NASA developed a new aircraft configuration called the STARC-ABL—single-aisle turbo-electric aircraft with an aft boundary layer propulsor—that incorporated BLI into an otherwise conventional configuration by adding a propulsor mounted on the tip of the tail cone. This aircraft is designed to cruise at Mach 0.72 and 37,000 ft with a wing area of 1400 ft². A rendering of this aircraft configuration is shown in Fig. 1. STARC-ABL uses a turbo-electric propulsion system with wing-mounted turbofan engines that also include electric generators to provide power to an electric motor powering the BLI propulsor.



Figure 1. NASA's STARC-ABL aircraft concept, incorporating a hybrid-electric propulsion system and aft-mounted BLI propulsor [4]

In their initial design study, Welstead and Felder [4] conclude that this configuration could offer up to a 12% reduction in fuel burn compared to the same configuration with a conventional propulsion system. For that study, the authors assume that the BLI propulsor would always run with a fixed power input of 3,500 hp, regardless of the flight speed, altitude, or throttle setting of the engine (except at very low throttle settings, where the power requirement was relaxed). Their propulsor had a FPR of 1.2, and an adiabatic efficiency of 95.6%.

The total thrust of STARC-ABL under-wing engines lapse more severely with altitude when compared to a conventional configuration, because they must provide a fixed amount of power to the BLI propulsor. The fixed power

off-take is a smaller percentage of the overall shaft power on the low-speed spool at lower altitudes. The fixed shaft power to the BLI propulsor also means that at low altitudes—such as take-off—the BLI propulsor does not provide as significant a portion of the overall thrust. However, as the aircraft climbs, the BLI propulsor’s share of the overall thrust increases as well. According to Welstead and Felder [4], the BLI propulsor provides only 20% of the overall thrust during take-off, but towards the end of the climb it provides 44%. This means that the performance of the propulsor is much more important at cruise than during take-off and climb.

The large share of thrust generated by the BLI propulsor at cruise is ultimately what enables the significant mission fuel burn reduction for this configuration. Therefore, the design of this propulsor is crucial to the overall performance and viability of the STARC-ABL concept. However, as previously explained, designing a BLI propulsor is challenging because of the tight coupling between the propulsion and aerodynamics disciplines.

In this work, we take a step towards fully coupled BLI propulsor design optimization by performing a coupled analysis of a simplified geometry—an axisymmetric fuselage with no wings at zero angle of attack. Although this simplified geometry cannot be considered an aircraft configuration since it would not fly, it represents the simplest case where we can capture the primary interdisciplinary interactions for a BLI propulsor on the STARC-ABL configuration. A profile view of the simplified configuration, along with key dimensions is shown in Fig. 2.

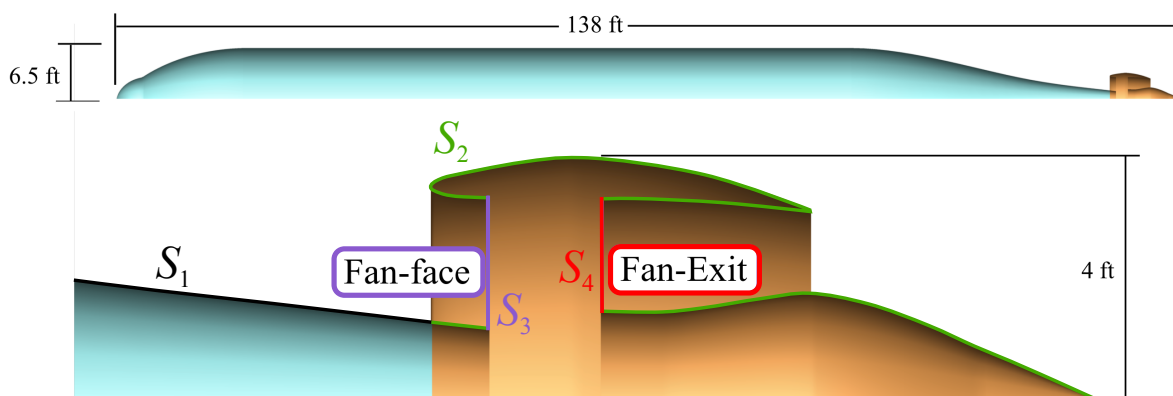


Figure 2. Axisymmetric fuselage with aft mounted BLI propulsor representing a simplified STARC-ABL configuration.

III. Modeling

A. Propulsion Model

The BLI propulsor is modeled using the 1D thermodynamic cycle analysis tool pyCycle [34, 35]. pyCycle, which is developed using OpenMDAO, allows for flexible modeling of propulsion systems by providing a library of different cycle elements (inlet, compressor, combustor, nozzle, and duct) that can be combined to model a specific propulsion system. pyCycle also computes adjoint analytic derivatives, which will enable design optimization with a fully coupled aero-propulsive adjoint in future work.

The propulsor model in the present work is comprised of a single compressor representing the fan. The model inputs are FPR, and total temperature and pressure at the fan-face. The outputs are the total temperature and pressure at the fan exit, and the mass flow rate for the fixed shaft power of 3,500 hp. Welstead and Felder [4] selected 3,500 hp in their original work by sizing their propulsor to capture about 70% of reduced speed air. The justification for this choice was based on their analysis, which indicated that increasing the propulsor power beyond that level would achieve only marginal gains. For this work, we keep this same propulsor power, but in future work we will allow this to vary.

The fan adiabatic efficiency (η_a) is computed as a function of FPR. At a lower FPR, less flow turning is required, and hence a higher adiabatic efficiency can be achieved. We assume the following linear relationship between η_a and FPR,

$$\eta_a = 1.066 - 0.0866\text{FPR} , \quad (1)$$

where the constants were chosen to give 96.2% efficiency at a FPR=1.2 and 95% efficiency at FPR=1.4.

B. BLI Aerodynamic Model

The aerodynamic model uses the RANS solver ADflow [25, 24], which is an efficient viscous adjoint with an in-memory interface to Python that greatly simplifies the integration with OpenMDAO. The axisymmetric geometry of our simplified geometry allows us to use a small structured multiblock mesh with 170,000 cells to capture the relevant physics. On a desktop computer with a 3.6 GHz, 4 core, Intel core-I7 processor and 8 GB of memory, this mesh can be converged 10 orders of magnitude in approximately 2 minutes.

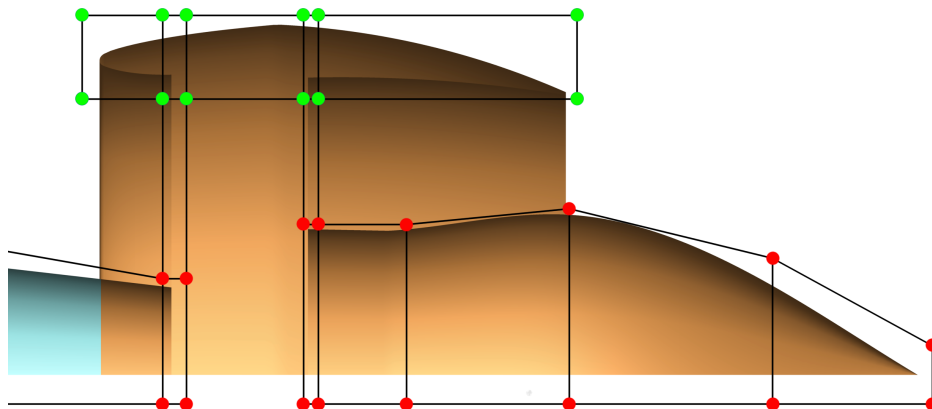


Figure 3. Free-form deformation defining the geometry parametrization. Green nodes are allowed to move while red nodes are fixed.

The fuselage for our model was designed to be similar to that of a Boeing 737-900 in length and diameter. A free-form deformation (FFD) approach [36] was used to parameterize the BLI propulsor diameter. This was accomplished by defining an FFD that rigidly translates the top of the nacelle up or down to scale the propulsor. Figure 3 shows the layout of the FFD boxes that parameterize the geometry, where the green nodes are the corners of the boxes that translate up and down to scale the nacelle diameter. The red nodes are held fixed to maintain the fuselage and nozzle plug geometry. In future work, additional control points will be added, and both red and green nodes will be able to move to perform more detailed shape optimization.

The propulsion-related inputs to our model are the diameter of the nacelle (d_{nac}) and the two boundary conditions that account for the fan: fan-face and fan-exit boundary conditions, as shown in Fig. 2. At the fan-face, we apply an outflow boundary condition (flow leaving the CFD domain), where the static pressure is specified. At the fan exit, we apply an inflow boundary condition, where the total pressure and temperature are specified.

We compute the net horizontal force on the body, F_x , by integrating the pressure and viscous forces on all solid surfaces, and the pressure and momentum flux contributions on the fan-face and fan exit, where all the contributions are resolved in the x -direction. This integration can be written as follows:

$$F_x = \underbrace{\iint_{S_1} (p\hat{n} + \mathbf{f}_{visc}) \cdot \hat{x}dS}_{F_{fuse}} + \underbrace{\iint_{S_2} (p\hat{n} + \mathbf{f}_{visc}) \cdot \hat{x}dS - \iint_{S_3} \rho_3 u_3^2 dS + \iint_{S_4} \rho_4 u_4^2 dS}_{F_{prop}}, \quad (2)$$

where S_1 is the portion of the fuselage surface shown in blue in Fig. 2, S_2 is the aft portion of the body shown as the green outline, S_3 represents the fan-face (purple), and S_4 is the fan exit (red). As indicated in this equation, we decompose the total force into F_{fuse} and F_{prop} . We do this decomposition to facilitate the discussion of our results, but this does not imply that fuselage drag, nacelle drag, and thrust can be neatly separated. Neither of these quantities are integrated over a closed control volume and therefore they do not represent true body forces. Furthermore, for a BLI configuration, thrust and drag are no longer independent quantities that can be separated in a meaningful way.

As part of our modeling, we also integrate the mass flow rates across both the fan-face and fan exit, and the mass-averaged total properties at the fan-face. Taking a mass-average of the total properties, as apposed to an arithmetic-average or area-average, is important for keeping a conservative data transfer between the aerodynamic and propulsion analyses.

C. Podd Configuration Aerodynamic Model

To provide a consistent point of reference modeled with the same tools and assumptions as the BLI configuration, we constructed an aerodynamic model that emulates a conventional podded configuration. This model consists of two separate simulations: one for the clean fuselage, and another for the podded propulsor, as shown in Fig. 4.

For this decoupled configuration, we can assume that the aerodynamic performance of the fuselage and the propulsor are independent of each other. Using the clean fuselage, we can compute a baseline F_{fuse} , and then the F_x of the podded configuration can be found by adding F_{fuse} and F_{prop} from a converged simulation of the independent propulsor.

Other than replacing the fuselage with a rounded spinner in the podded propulsor model, the geometry of the nacelle and boundary conditions of the BLI aerodynamic model are identical to those of the podded one. This allows the same FFD parameterization to be used for both models, and it also means that the same coupling scheme can be used for both the BLI and podded configurations.

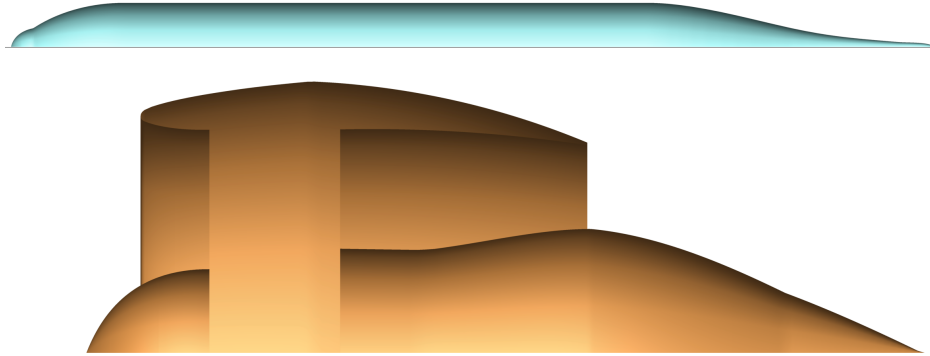


Figure 4. Podded propulsor configuration with clean fuselage (top) and detailed view of the propulsor (bottom).

D. Fully Coupled Model

Before we describe the coupling method used in this work, we should clarify what we mean by “coupled” and “uncoupled”. We define a coupled model to be one where data is passed between two or more analyses in a reciprocal manner, so that some form of iteration (manual or automatic) between the analyses is performed to reach overall physical compatibility. We define uncoupled analysis to be one in which data is passed through sequentially from one model to another, requiring only one solution for each model.

There has been some recent work developing coupled aero-propulsive models for supersonic applications. Heath et al. [37] manually coupled a RANS analysis to a propulsion model by matching the flow areas and states between the two, and by using the propulsion model to predict the static pressure for the fan-face boundary condition. They compared the installed performance and sonic boom for two discrete inlet designs, and the limited number of configurations made manual coupling a reasonable approach. Connolly et al. [20] developed a transient coupled model using an Euler aerodynamic model and 1D gas-dynamics propulsion model for aero-propulso-servo-elasticity applications. They iterated by passing boundary condition values at the interfaces between the two models at every time step to compute state derivatives for the time integration.

Our work uses a similar scheme to that of Connolly et al. [20], where thermodynamic states are exchanged by the two models. However, our method differ in key implementation details. Their implementation integrates the propulsion model directly into the aerodynamic solver, including the coupling terms as additional state variables to be converged with the rest of the simulation. Our method relies on the OpenMDAO framework to manage the multidisciplinary analysis and converge the simulation [33]. This approach is less intrusive because it requires no modifications to either analysis code, allowing for a more complex solver structure.

The fully coupled aero-propulsive simulation was built with a two-level solver scheme shown in Fig. 5, which was used for both podded and BLI configurations. The top level is converged by a nonlinear Gauss–Seidel solver that manages three residuals defined by the following coupling variables: fan-face total pressure (\bar{p}_t^{FF}), fan-face total temperature (T_t^{FF}), and propulsor mass flow rate (\dot{m}^{prop}). The inner level is converged using a Broyden solver that handles two additional residuals: $\mathcal{R}_{p_s}^{\text{FF}}$ and $\mathcal{R}_{d_{\text{nac}}}$. The mass flow rate between the fan-face and fan-exit boundary conditions is balanced by varying fan-face static pressure (p_s^{FF}) to converge the static pressure residual:

$$\mathcal{R}_{p_s}^{\text{FF}} = \dot{m}^{\text{FF}} - \dot{m}^{\text{FE}}. \quad (3)$$

The mass flow rate between the aerodynamic and propulsion simulations is balanced by varying the nacelle diameter (d_{nac}) to converge the nacelle diameter residual:

$$\mathcal{R}_{d_{\text{nac}}} = \dot{m}^{\text{prop}} - \dot{m}^{\text{FE}}. \quad (4)$$

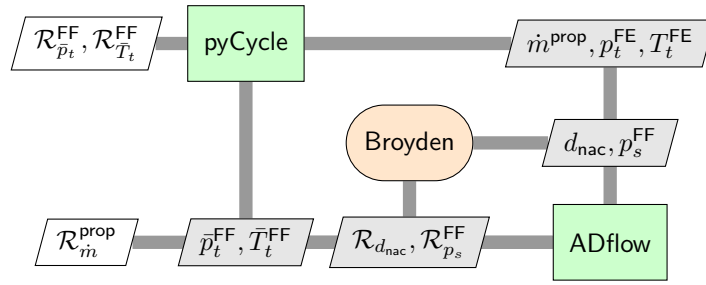


Figure 5. XDSM [38] for the coupled aero-propulsive analysis.

This last residual is formulated based on the assumption of a fixed input shaft power of 3,500 hp. This assumption provides a convenient way to compare different propulsor designs. Since they both have the same amount of input power, the configuration that provides the highest overall F_x is the most efficient.

Note that an alternate reference point is also possible for which the power (and hence \dot{m}^{prop}) would be varied to achieve steady flight ($F_x = 0$). In this case, the design with the lowest power input to the propulsor would be the most efficient. Ultimately, this approach was discarded because part of the STARC-ABL thrust is produced by the under-wing engines. It is not yet clear what the best thrust split between the under-wing engines and BLI propulsor would be, and the fixed-power scheme lends itself more naturally to a problem formulation with a variable thrust split.

IV. Results

We conducted a trade study by performing a parameter sweep of FPR from 1.2 to 1.35, and then comparing the performance of the podded configuration to that of the BLI configuration. For the podded configuration, we assume that changes to the fuselage only affect F_{fuse} , and changes to the propulsion system only affect F_{prop} . With BLI, this assumption is no longer valid, and the performance metric is based on the net force in the axial direction (F_x) on the combined fuselage-propulsor system. However, it is still useful to examine F_{prop} and F_{fuse} to understand how these quantities vary across the propulsor design space, and how the net performance is achieved.

All forces are nondimensionalized as follows:

$$C_F = \frac{2F}{\rho_\infty V_\infty^2 A_{\text{ref}}}, \quad (5)$$

where A_{ref} is the reference wing area for the STARC-ABL aircraft. The values used in the nondimensionalization are listed in Table 1. This table includes a reference length, l_{ref} , whose value is the baseline outer nacelle radius and will be used to nondimensionalize the coordinates in the boundary layer.

In our convention, the sign of the force indicates the direction of action: Positive values represent forward force that would cause acceleration, while negative values represent backward force that would cause deceleration. Note that we retain this sign convention even when breaking F_x into F_{prop} and F_{fuse} , so it is expected that the F_{prop} be positive and F_{fuse} be negative.

Table 1. Reference values used in the nondimensionalization.

p_∞	3.834 psi
ρ_∞	0.0008 slug/ft ³
V_∞	707.3 ft/sec
A_{ref}	1,400 ft ²
l_{ref}	4 ft

When working with force coefficients it is common to refer to *counts of force*, which correspond to $10^4 \times C_F$. The results presented below show that the BLI system outperforms the conventional podded configuration by at least 5 force counts across the range of FPR designs considered, and that the aerodynamics and the propulsive improvements

both contribute equally to the gains. Thus, a fully coupled analysis is necessary to accurately capture the full BLI effect.

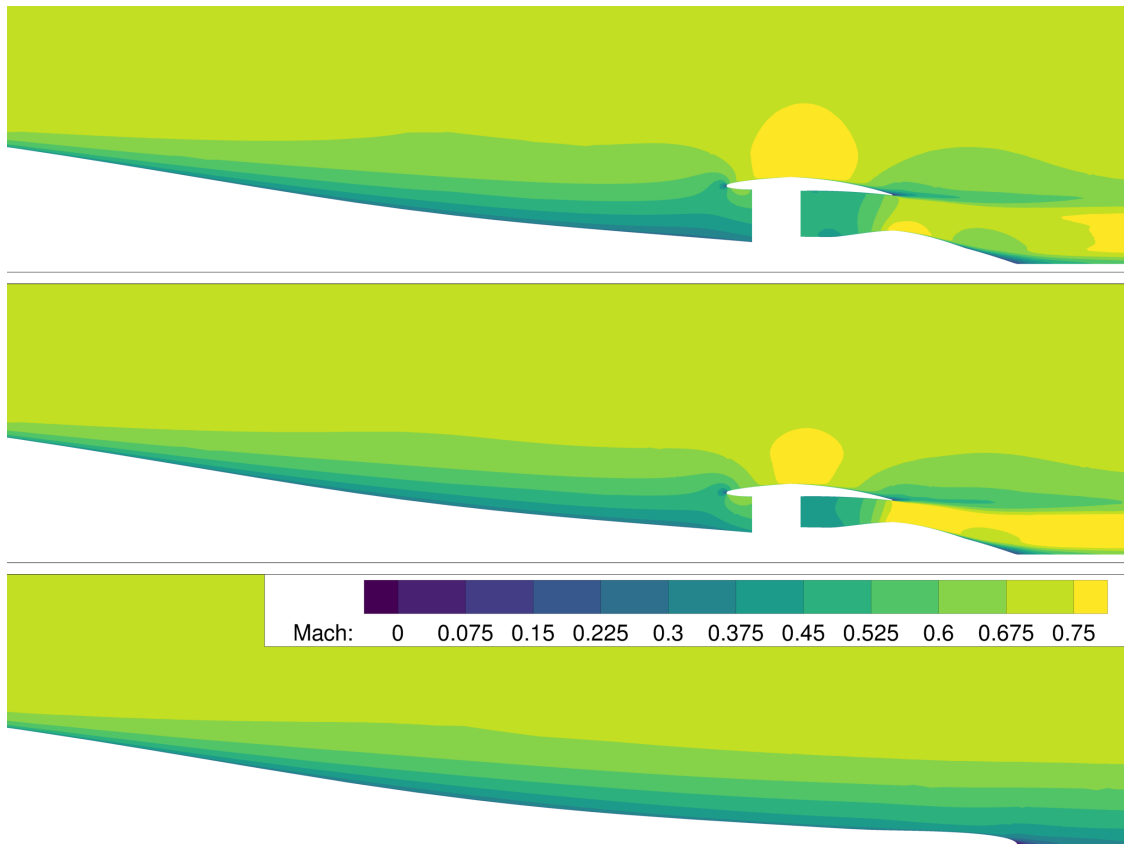


Figure 6. Converged flow solutions for FPR = 1.2 (top), FPR = 1.35 (middle), and the clean fuselage (bottom) designs

The aerodynamic benefit of the BLI configuration is shown qualitatively in Fig. 6, which plots contours of Mach number. The bottom image represents the clean fuselage, the middle one is a BLI configuration with FPR = 1.35, and the top one is a BLI configuration with FPR = 1.2. As the FPR is reduced for a fixed input power to the fan, the mass flow rate increases, requiring a larger nacelle. The diameter of the nacelle has a strong influence on the height of the boundary layer on the aft fuselage. The largest nacelle, for FPR = 1.2, also has the thickest boundary layer. The boundary layer heights (δ) measured at the nacelle lip for the three configurations are listed in Table 2. The boundary layer grows 15% between the podded configuration and the FPR = 1.35 BLI configuration, while for the FPR = 1.2 design it grows by 25%. This variation in the boundary layer profile as a function of the nacelle design demonstrates a sensitivity of the aerodynamics with respect to the propulsion design variable (FPR).

Table 2. Boundary layer height at the nacelle lip for podded and BLI configurations.

Configuration	δ (ft)	Change
Podded	4.0	0 %
BLI with FPR = 1.35	4.6	15%
BLI with FPR = 1.20	5.0	25%

A. Net force as a function of FPR

The calculation of C_{F_x} must be handled slightly differently for the podded and BLI configurations. For the podded configuration, the force on the fuselage is constant and is independent of any changes to the pod. Therefore, the contribution of the fuselage can be computed at the given flight condition, and then combined with the contribution

from the podded propulsor for any given FPR as follows:

$$C_{F_x} = C_{F_{prop}} + C_{F_{fuse}}, \quad (6)$$

where $C_{F_{fuse}} = -0.008321$.

For the BLI configuration, we compute the net force integration on the whole wetted surface, and fan-face and fan exit, as detailed in Eqn. (2). A comparison of C_{F_x} between the podded and BLI configurations is plotted in Fig. 7. The primary conclusion from Fig. 7 is that BLI offers an additional 24 to 27 of net force counts. That represents a 33% increase relative to the conventional podded configuration. The data also shows two key trends: first, for the podded configuration net force is insensitive to FPR; and second, the BLI configuration clearly performs better at lower FPR designs. We can gain further insight into these trends by breaking C_{F_x} down into $C_{F_{fuse}}$ and $C_{F_{prop}}$ to look at the contributions from each discipline.

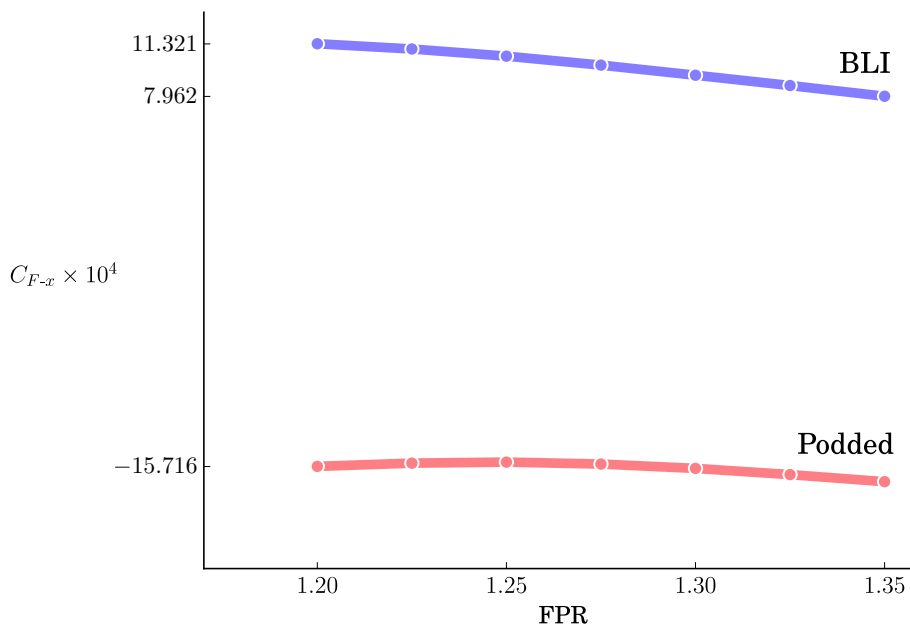


Figure 7. Net force on the body (fuselage and propulsor) as a function of design FPR.

B. Propulsor force as a function of FPR

Figure 8 shows the variation of the propulsor force with FPR for both podded and BLI configurations. For the podded configuration, where F_{fuse} is constant, the variation in C_{F_x} is solely due to changes in F_{prop} at different FPR designs. Figure 8 shows that there is only a 1.4 force count variation in F_{prop} as a function of FPR for the podded configuration. This result might be surprising if viewed from a purely thermodynamic perspective. Thermodynamics would predict that F_{prop} would increase as the FPR is lowered due to higher propulsive efficiency and a higher adiabatic efficiency—defined by Eqn. (1). However, the coupled analysis accounts for both thermodynamic and aerodynamics effects. While the net thrust does go up, the nacelle drag also increases by nearly as much, and hence, the net effect is a fairly flat response, with slightly better performance near FPR = 1.25.

The drag increases for lower FPR designs because there is a stronger shock on the outer surface of the nacelle for the larger nacelles, as seen in Fig. 9. The presence of that shock in both configurations indicates that the nacelle geometry is not ideal. In fact, we can see that the same effect is present for the BLI configuration by looking at Fig. 6, where the area of high speed flow is larger for the FPR = 1.2 configuration on top. Although we would normally expect the larger nacelle with a correspondingly larger fan to have more drag, it is possible that some of the adverse effects are mitigated by a better geometry. Future work will use shape optimization to allow for optimal inlet nacelle shaping for each design. However, since this suboptimal inlet design is used for all the cases presented herein, our performance comparison is still valid.

The propulsor force trend for the BLI configuration in Fig. 8 is different from the trend in Fig. 7. For FPR = 1.35, the BLI configuration outperforms the podded configuration by 15.8 force counts. For FPR = 1.2, the difference is

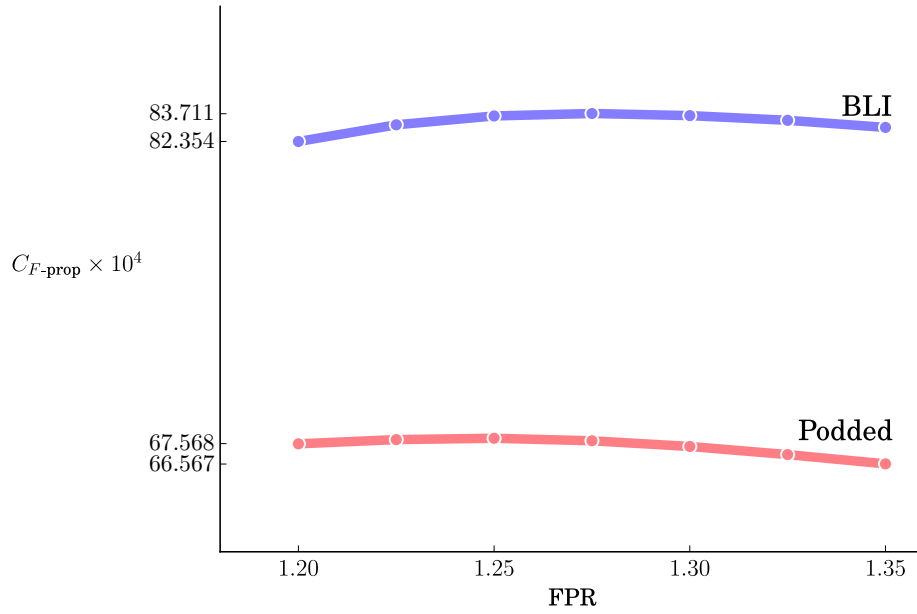


Figure 8. Force integrated over propulsor ($C_{F_{prop}}$) as a function of design FPR.

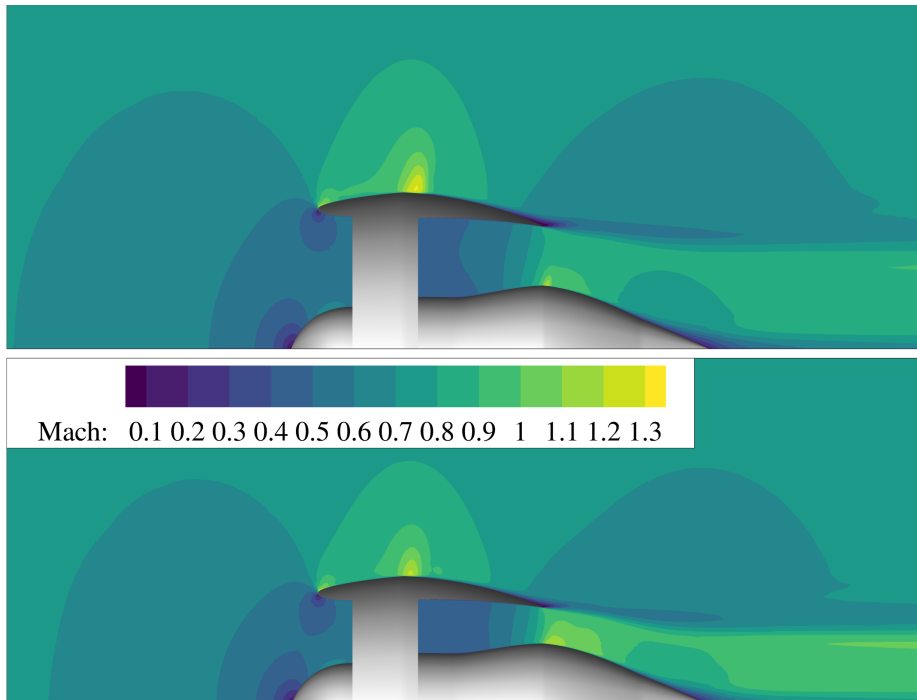


Figure 9. Mach contours for the propulsor simulation on the FPR = 1.2 (top) and FPR = 1.35 (bottom) designs of the podded configuration.

16.1 force counts. Although this variation is small, it is still opposite of the variation of C_{F_x} with FPR. This BLI trend occurs because as the nacelle grows, the BLI benefit decreases since a larger percentage of freestream flow is ingested, which results in increased ram drag. Hence, the BLI benefit to the propulsion system becomes less pronounced for lower FPR designs. Additionally, by comparing Fig. 7 with Fig. 8, we see that only considering the BLI effect on the propulsion analysis would both underpredict the benefit by between 27% and 36%, and result in a different optimal FPR value.

The difference in magnitude and trend between $C_{F_{prop}}$ and C_{F_x} highlights the importance of using a fully coupled analysis to study BLI. Another important difference between the uncoupled and coupled modeling can be seen by examining the mass-averaged fan-face total pressure, which is defined as

$$\bar{p}_t^{FF} = \frac{\int_0^{d_{nac}} p_t(y) \dot{m}(y) dy}{\int_0^{d_{nac}} \dot{m}(y) dy}. \quad (7)$$

For an uncoupled analysis, where we assume that the aerodynamics are unchanged from the podded configuration, $p_t(y)$ and $\dot{m}(y)$ in Eqn. 7 are extracted from the boundary layer profile of the clean fuselage in the podded configuration, and are independent of any propulsion design variable. Therefore, for uncoupled analysis, \bar{p}_t^{FF} only depends on the nacelle diameter. This type of analysis was used by Welstead and Felder [4] in their study of the STARC-ABL configuration, and by Liu et. al [16] and Laskaridis et al. [17] in their studies of a HWB turbo-electric distributed propulsion configuration.

When the analysis is fully coupled, p_t^{FF} and \dot{m} are not only a function of the nacelle diameter, but a function of the propulsor design as well, through the FPR.

Figure 10 compares \bar{p}_t as a function of FPR between podded configuration and the BLI configuration. The BLI results are computed using both uncoupled, and coupled analyses. For the podded configuration, \bar{p}_t^{FF} is independent of FPR, since the inlet just ingests from the freestream. The BLI configuration uncoupled analysis (dashed blue line), does capture the inverse relationship of \bar{p}_t^{FF} with FPR, but it overpredicts \bar{p}_t^{FF} by between 4% and 6% compared to the coupled method (solid blue line).

This overprediction is significant: For an electrically driven propulsor, a 5% lower \bar{p}_t means a that the nozzle pressure ratio decreases by the same percentage, and the result is a similar decrease in thrust. This effect would be even more pronounced for a BLI design using a conventional turbofan, where the additional total pressure loss would have a direct impact on the overall pressure ratio and thermal efficiency of the engine. Thus, it is crucial to consider the aerodynamic changes caused by the presence of the propulsor using a coupled analysis.

C. Fuselage force as a function of FPR

Figure 11 shows the aerodynamic contribution to the overall performance. The podded data is constant by definition, since there is no aerodynamic interaction between the propulsor and the fuselage. The BLI configuration has better $C_{F_{fuse}}$ for all designs by at least 8.2 force counts. However, unlike the forces on the propulsor, $C_{F_{fuse}}$ for the BLI configuration exhibits a strong variation with FPR. From the FPR = 1.35 design to the FPR = 1.2 design, the $C_{F_{fuse}}$ improves by an additional 4.0 counts. The total variation in $C_{F_{fuse}}$ is larger than the total variation in $C_{F_{prop}}$ observed in Fig. 8, indicating that the aerodynamic performance is more sensitive to FPR—a propulsor design variable—than to the propulsor performance.

The sensitivity of the aerodynamics to FPR in the BLI configuration is due to variations in the flow field in the aft fuselage. We can see this effect qualitatively in Fig. 6. The actual velocity profiles for the podded configuration, and the BLI configuration for FPRs of 1.35 and 1.2 are shown in Fig. 12, where all distances are normalized by the baseline nacelle outer radius, $l_{ref} = 4$ ft. We see that the propulsor slows down the flow near the surface, and that this effect extends to about one nacelle radius forward of the fan-face. Also, the larger propulsor for the FPR = 1.2 design has a more significant impact on the flow than the smaller propulsor for FPR = 1.35.

The boundary layer profiles demonstrate that the flow on the aft fuselage is influenced by the aft propulsor, and hence provide an aerodynamic justification for the results shown in Fig. 10. These profiles explain why the coupled analysis predicts a lower p_t^{FF} than the uncoupled analysis. Even for the uncoupled analysis, the dashed-blue line in Fig. 10 shows a loss of total pressure that varies with FPR, and thus with nacelle diameter as well. However, the uncoupled analysis assumes that the boundary layer velocity profile is fixed and independent of the propulsor design. The fully coupled analysis captures the change in the boundary layer as the propulsor diameter changes, which further lowers the total pressure compared to what the uncoupled analysis predicts. The lower flow speeds in the boundary layer might also partially explain the reduced $C_{F_{prop}}$ in the BLI configuration. However, the difference in boundary layer profiles only propagates about one nacelle radius forward, and qualitatively does not seem to indicate a significant reduction in viscous losses to justify the full effect seen in $C_{F_{prop}}$.

To better understand the aerodynamic cause for the change in $C_{F_{prop}}$, we examined the C_p distribution on the surface of the aft fuselage. Figure 13 confirms that there is a significant difference in the pressure along the aft fuselage, but it also shows that the effect reaches farther upstream on the fuselage than the variation in boundary layer profiles. The C_p near the fan-face changes by 50%, but even at 3.5 nacelle radii away from the inlet, there are still differences in the C_p . Hence, the surface pressure effects of the BLI propagate much farther forward than the changes in the velocity profile would suggest. Even small variations in C_p can have a large effect on the body forces, since they act over a

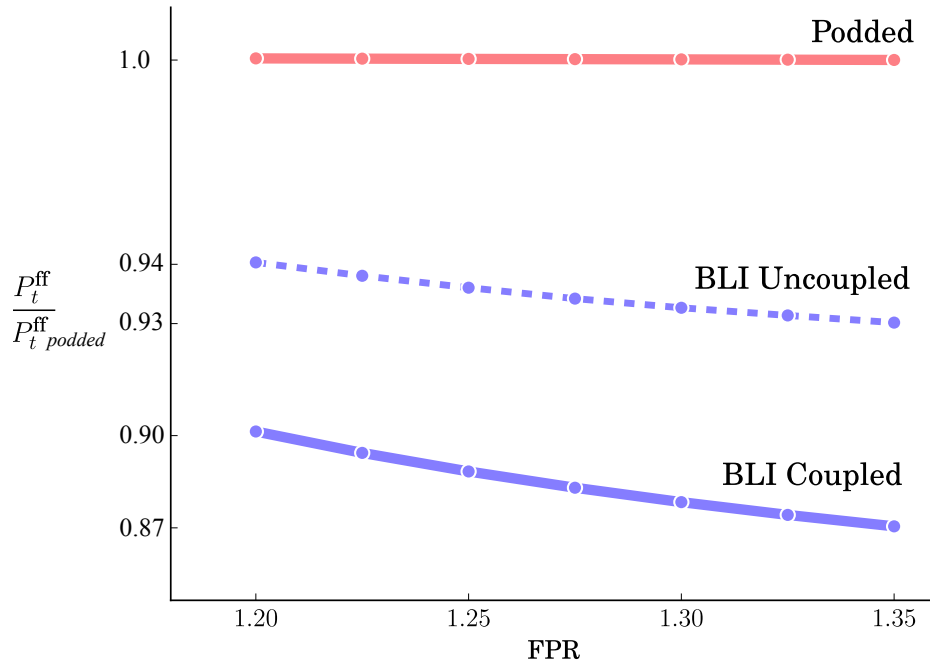


Figure 10. Mass-averaged total pressure normalized by the value for the podded configuration as a function of FPR for the podded configuration (pink), the BLI configuration with a fully coupled analysis (solid blue), and a decoupled analysis (dashed blue)

large area. The pressure distribution shown in Fig. 13 explains the trend for the BLI configuration in Fig. 11. As the FPR decreases and the propulsor increases in diameter, the effect of the higher pressure at the fan-face propagates farther upstream and further decreases $C_{F_{prop}}$.

The trends in Fig. 13 summarize the most significant finding of this work: The presence of the propulsor in a BLI configuration can have a large impact on the pressure distribution along the aerodynamic surface it is attached to. Furthermore, we can see that the details of that interaction are highly sensitive to changes in the propulsor design and

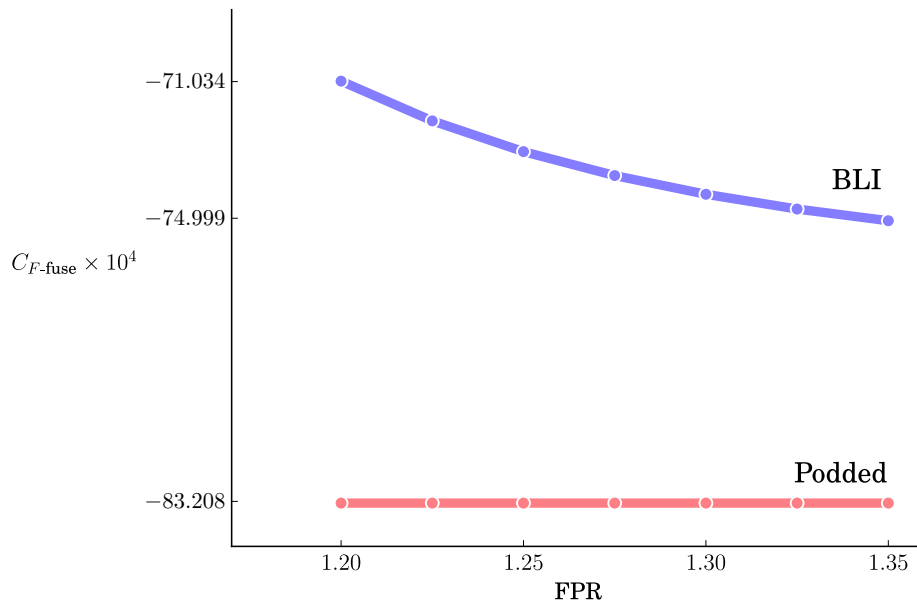


Figure 11. Force coefficient on the fuselage, $C_{F_{fuse}}$ as a function of design FPR.

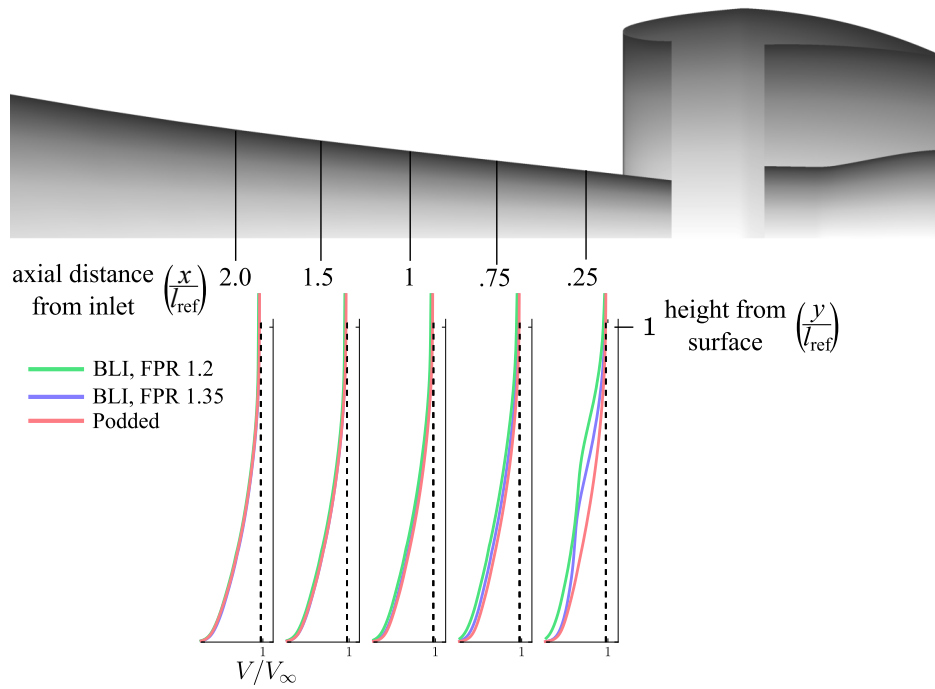


Figure 12. Comparison of boundary layer profiles at the aft fuselage between the podded and BLI configurations; $l_{ref} = 4ft$.

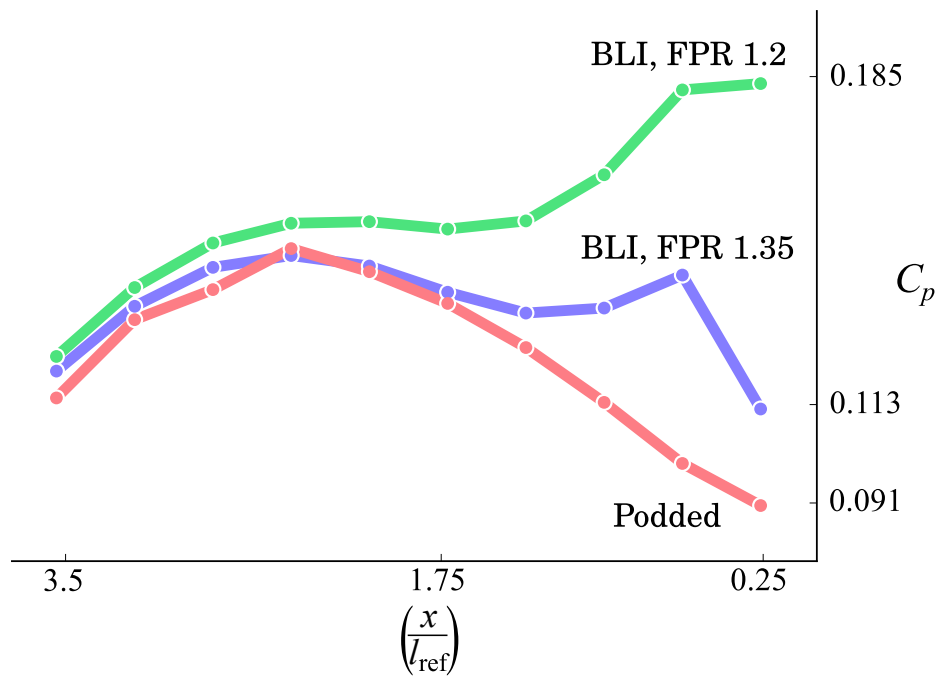


Figure 13. Comparison of surface C_p vs axial distance from the inlet (x/l_{ref}) between the podded and BLI configurations vs axial distance with FPRs of 1.35 and 1.2; $l_{ref} = 4ft$.

shaft input power, which affects the static pressure distribution.

Our results show that there is an inverse relationship between the change in the mean static pressure on the fuselage and FPR, but this relationship could be altered by varying other aspects of the propulsor design not considered here. The fan-face static pressure—which affects the static pressure distribution on the aft fuselage—is a function of both throttle setting and inlet design. Throttling down would increase the fan-face static pressure and thus mean static pressure, while throttling up would decrease it. Even for a fixed FPR and throttle setting, the inlet design could still allow an extra degree of design freedom. By making the inlet more or less diffusive you can alter the interdisciplinary coupling between the fan-face static pressure and the aft fuselage static pressure distribution. Such inlet design changes would have an impact on propulsor performance, but the multidisciplinary effects would allow aero-propulsive trades to seek highest overall system efficiency.

V. Conclusions

We presented a new approach for building coupled aero-propulsive analyses of BLI propulsion systems using a 1D cycle model and a RANS aerodynamic model. The approach was implemented in the OpenMDAO framework, using pyCycle and ADflow for the propulsion and aerodynamic analyses, respectively. A simplified version of NASA's STARC-ABL configuration was modeled, and a parameter sweep of propulsor FPR from 1.2 to 1.35 was performed to study the coupled performance of the aft-mounted BLI propulsor and characterize the contributions from each discipline.

The coupled analysis shows that BLI offers at least 24 force counts of increased performance relative to the podded configuration across the FPR range. This represents a 23% increase in thrust relative to the 67 force counts of thrust for the podded configuration, which clearly demonstrates the large potential for performance improvement due to BLI in this configuration.

The trends were further analyzed by breaking the net force down into aerodynamic and propulsive contributions. The breakdown of the improvements shows that 8 to 12 force counts were due to aerodynamics and 16 counts were due to propulsion. Thus, the BLI configuration benefits from aerodynamics and propulsion are essentially of equal importance. These results demonstrate the need for a fully coupled model to predict the performance of the BLI configuration, since considering only propulsion or only aerodynamics would only achieve a fraction of the possible improvement.

The BLI benefit to the propulsion system arises primarily from a decrease in incoming momentum flux (a reduction in ram drag). The thrust data presented here shows that this benefit is only a weak function of FPR because of the offsetting thermodynamic improvements and nacelle drag increases. It is possible that a more refined nacelle geometry would alleviate some of the drag penalties for the lower FPR designs shown here, and thus change the trend with respect to FPR, but the general effect of decreased ram drag would persist.

The BLI benefit to the aerodynamics was due to higher mean static pressure along the aft section of the fuselage relative to the clean fuselage in the podded configuration, and this higher pressure was caused by the influence of the BLI fan. In the podded configuration the fan-face static pressure is higher than the local static pressure on the aft section of the clean fuselage. When the propulsor is moved down onto the fuselage the relatively higher fan-face static pressure is able to favorably alter the mean static pressure on the aft-fuselage without adversely affecting the pressure forces on the propulsor.

The reduced ram-drag on the propulsor combined with the increased mean static pressure along the aft fuselage combine to create the mutually beneficial affects in the BLI configuration. While the propulsion effect was slightly larger in magnitude, the aerodynamic effect was far more sensitive to FPR. This occurred because, with a fixed input shaft power, the FPR effectively determines the nacelle diameter (i.e., a lower FPR means a larger nacelle). The diameter of the nacelle had a direct effect on how far upstream the BLI effects propagated and meant that lower FPR designs had a much larger aerodynamic effect and a strong multidisciplinary coupling.

The variation in pressure along the surface of the aft fuselage indicates that BLI propulsion systems can have a strong impact on the static pressure distribution of the associated aerodynamic surfaces. For the STARC-ABL configuration, this yields a decrease in drag, but other configurations, such as the MIT D8 or the turbo-electric distributed propulsion HWB, could potentially see additional aerodynamic effects. For these aircraft, the variation in the surface pressure caused by the BLI propulsion system could cause not only propulsion-dependent drag effects, but also lift and pitching moments. This means that BLI could ultimately result in throttle-dependent angle of attack and trim settings.

The overall performance of the BLI configuration depends heavily on both propulsion and aerodynamic performance and each discipline strongly impacts the other. Both propulsion and aerodynamic performance are impacted by design choices from the other discipline. In this work, we considered only a single propulsor design variable(FPR). However, given the strength of the coupling demonstrated by the results the overall performance is likely to be sen-

sitive to other variables, such as fuselage geometry, nacelle geometry, inlet design, and shaft input power. Therefore, to achieve optimal overall performance, a careful balance between aerodynamic and propulsive considerations is required. We will address this in future work, where we will refine this concept using design optimization with a gradient-based algorithm and coupled-adjoint analytic derivatives to simultaneously optimize propulsion and aerodynamics design variables.

Acknowledgments

The authors would like to acknowledge Bret Naylor, Kenneth Moore, and the rest of the NASA Glenn OpenM-DAO development team, who have spent countless hours building the framework that has enabled this research. We would also like to thank James Felder, of the NASA Glenn Research Center, for lending his time and expertise to many discussions regarding the propulsion system design of the STARC-ABL configuration. We also gratefully acknowledge NASA's Aeronautics Research Mission Directorate Transformational Tools and Technologies (TTT) and the Advanced Air Transport Technologies (AATT) projects for their continued support of this work.

References

- [1] Betz, A. and Albring, W., "Introduction to the Theory of Flow Machines," *ZAMM - Journal of Applied Mathematics and Mechanics / Zeitschrift für Angewandte Mathematik und Mechanik*, Vol. 47, No. 2, 1967, pp. 140–141. doi:[10.1002/zamm.19670470224](https://doi.org/10.1002/zamm.19670470224).
- [2] Wislicenus, G. F., "Hydrodynamics and Propulsion of Submerged Bodies," *Journal of the American Rocket Society*, Vol. 30, December 1960, pp. 1140–1148.
- [3] Gearhart, W. S. and Henderson, R. E., "Selection of a Propulsor for a Submersible System," *Journal of Aircraft*, Vol. 3, No. 1, 1966, pp. 84–90.
- [4] Welstead, J. R. and Felder, J. L., "Conceptual Design of a Single-Aisle Turboelectric Commercial Transport with Fuselage Boundary Layer Ingestion," *54th AIAA Aerospace Sciences Meeting*, AIAA 2016-1027, 2016. doi:[10.2514/6.2016-1027](https://doi.org/10.2514/6.2016-1027).
- [5] Felder, J. L., Kim, H. D., and Brown, G. V., "Turboelectric Distributed Propulsion Engine Cycle Analysis for Hybrid-Wing-Body Aircraft," *47th AIAA Aerospace Sciences Meeting including The New Horizons Forum and Aerospace Exposition*, AIAA 2009-1132, 2009. doi:[10.2514/6.2009-1132](https://doi.org/10.2514/6.2009-1132).
- [6] Daggett, D. L., Kawai, R., and Friedman, D., "Blended Wing Body Systems Studies: Boundary Layer Ingestion Inlets With Active Flow Control," Tech. Rep. NASA/CR-2003-212670, NASA Langley Research Center, December 2003.
- [7] Smith, A. M. O. and Roberts, H. E., "The Jet Airplane Utilizing Boundary Layer Ingestion for Propulsion," *Journal of Aeronautical Sciences*, Vol. 14, No. 2, 1947, pp. 97–109.
- [8] Smith, L. H., "Wake Ingestion Propulsion Benefit," *Journal of Propulsion and Power*, Vol. 9, No. 1, February 1993, pp. 74–82. doi:[10.2514/6.1991-2007](https://doi.org/10.2514/6.1991-2007).
- [9] Drela, M., "Power Balance in Aerodynamic Flows," *AIAA Journal*, Vol. 47, No. 7, 2009, pp. 1761–1771. doi:[10.2514/1.42409](https://doi.org/10.2514/1.42409).
- [10] Arntz, A., Atinault, O., and Merlen, A., "Exergy-Based Formulation for Aircraft Aeropropulsive Performance Assessment: Theoretical Development," *AIAA Journal*, Vol. 53, No. 6, 2015, pp. 1627–1639. doi:[10.2514/1.J053467](https://doi.org/10.2514/1.J053467).
- [11] Arntz, A. and Atinault, O., "Exergy-Based Performance Assessment of a Blended WingBody with Boundary-Layer Ingestion," *AIAA Journal*, Vol. 53, No. 12, 2015, pp. 3766–3776. doi:[10.2514/1.J054072](https://doi.org/10.2514/1.J054072).
- [12] Hardin, L., Tillman, G., Sharma, O., Berton, J., and Arend, D., "Aircraft System Study of Boundary Layer Ingesting Propulsion," *48th AIAA/ASME/SAE/ASEE Joint Propulsion Conference and Exhibit*, AIAA-2012-2993, 2012. doi:[10.2514/6.2012-3993](https://doi.org/10.2514/6.2012-3993).
- [13] Kim, H. and Liou, M.-S., "Optimal Inlet Shape Design of N2B Hybrid Wing Body Configuration," *Proceedings of the 48th AIAA/ASME/SAE/ASEE Joint Propulsion Conference and Exhibit*, AIAA-2012-3917, 2012. doi:[10.2514/6.2012-3917](https://doi.org/10.2514/6.2012-3917).
- [14] Kim, H. and Liou, M.-S., "Optimal Shape Design of Mail-Slot Nacelle on N3X Hybrid Wing-Body Configuration," *Proceedings of the 31st AIAA Applied Aerodynamics Conference*, AIAA-2013-2413, 2013. doi:[10.2514/6.2013-2413](https://doi.org/10.2514/6.2013-2413).
- [15] Blumenthal, B., Elmiligui, A. A., Geiselhart, K., Campbell, R. L., Maughmer, M. D., and Schmitz, S., "Computational Investigation of a Boundary-Layer Ingestion Propulsion System for the Common Research Model," *46th AIAA Fluid Dynamics Conference, Aviation Forum*, AIAA 2016-3812, 2016. doi:[10.2514/6.2016-3812](https://doi.org/10.2514/6.2016-3812).
- [16] Liu, C., Dougeris, G., Laskaridis, P., and Singh, R., "Thermal cycle analysis of turboelectric distributed propulsion system with boundary layer ingestion," *Aerospace Science and Technology*, Vol. 27, No. 1, 2013, pp. 163 – 170. doi:<http://dx.doi.org/10.1016/j.ast.2012.08.003>.
- [17] Laskaridis, P., Pachidis, V., and Pilidis, P., "Opportunities and challenges for distributed propulsion and boundary layer ingestion," *Aircraft Engineering and Aerospace Technology*, Vol. 86, No. 6, 2014, pp. 451–458. doi:[10.1108/AEAT-05-2014-0067](https://doi.org/10.1108/AEAT-05-2014-0067).
- [18] Jones, S., *An Introduction to Thermodynamic Performance Analysis of Aircraft Gas Turbine Engine Cycles Using the Numerical Propulsion System Simulation Code*, 2007, NASA TM-2007-214690.
- [19] Perullo, C., Trawick, D., Clifton, W., Tai, J. C., and Mavris, D. N., "Development of a suite of hybrid electric propulsion modeling elements using NPSS," *ASME Turbo Expo 2014: Turbine Technical Conference and Exposition*, 2014.
- [20] Joseph W. Connolly, Pawel Chwalowski, M. D. S. J.-r. C. W. A. S. J. J. M. and Kopasakis, G., "Towards an Aero-Propulso-Servo-Elasticity Analysis of a Commercial Supersonic Transport," *15th Dynamics Specialists Conference, AIAA SciTech Forum*, 2016. doi:<http://dx.doi.org/10.2514/6.2016-1320>.

- [21] Drela, M. and GILES, M., “Viscous-inviscid analysis of transonic and low Reynolds number airfoils,” *AIAA Journal*, Vol. 25, No. 10, 1987, pp. 1347–1355. doi:[10.2514/3.9789](https://doi.org/10.2514/3.9789).
- [22] Lock, R. C. and Williams, B. R., “Viscous-inviscid interactions in external aerodynamics,” *Progress in Aerospace Sciences*, Vol. 24, 1987, pp. 51–171.
- [23] Drela, M., “Three-Dimensional Integral Boundary Layer Formulation for General Configurations,” *21st AIAA Computational Fluid Dynamics Conference, Fluid Dynamics and Co-located Conferences*, AIAA 2013-2437, 2014. doi:[10.2514/6.2013-2437](https://doi.org/10.2514/6.2013-2437).
- [24] Lyu, Z., Kenway, G. K. W., and Martins, J. R. R. A., “Aerodynamic Shape Optimization Investigations of the Common Research Model Wing Benchmark,” *AIAA Journal*, Vol. 53, No. 4, April 2015, pp. 968–985. doi:[10.2514/1.J053318](https://doi.org/10.2514/1.J053318).
- [25] Lyu, Z., Kenway, G. K., Paige, C., and Martins, J. R. R. A., “Automatic Differentiation Adjoint of the Reynolds-Averaged Navier–Stokes Equations with a Turbulence Model,” *21st AIAA Computational Fluid Dynamics Conference*, San Diego, CA, Jul. 2013. doi:[10.2514/6.2013-2581](https://doi.org/10.2514/6.2013-2581).
- [26] Lyu, Z. and Martins, J. R. R. A., “Aerodynamic Design Optimization Studies of a Blended-Wing-Body Aircraft,” *Journal of Aircraft*, Vol. 51, No. 5, September 2014, pp. 1604–1617. doi:[10.2514/1.C032491](https://doi.org/10.2514/1.C032491).
- [27] Chen, S., Lyu, Z., Kenway, G. K. W., and Martins, J. R. R. A., “Aerodynamic Shape Optimization of the Common Research Model Wing-Body-Tail Configuration,” *Journal of Aircraft*, Vol. 53, No. 1, January 2016, pp. 276–293. doi:[10.2514/1.C033328](https://doi.org/10.2514/1.C033328).
- [28] Martins, J. R. R. A., Alonso, J. J., and Reuther, J. J., “High-Fidelity Aerostructural Design Optimization of a Supersonic Business Jet,” *Journal of Aircraft*, Vol. 41, No. 3, 2004, pp. 523–530. doi:[10.2514/1.11478](https://doi.org/10.2514/1.11478).
- [29] Martins, J. R. R. A., Alonso, J. J., and Reuther, J. J., “A Coupled-Adjoint Sensitivity Analysis Method for High-Fidelity Aero-Structural Design,” *Optimization and Engineering*, Vol. 6, No. 1, March 2005, pp. 33–62. doi:[10.1023/B:OPTE.0000048536.47956.62](https://doi.org/10.1023/B:OPTE.0000048536.47956.62).
- [30] Kenway, G. K. W., Kennedy, G. J., and Martins, J. R. R. A., “Scalable parallel approach for high-fidelity steady-state aeroelastic analysis and adjoint derivative computations,” *AIAA Journal*, Vol. 52, 2014, pp. 935–951. doi:[10.2514/1.J052255](https://doi.org/10.2514/1.J052255).
- [31] Kenway, G. K. W. and Martins, J. R. R. A., “Multipoint High-fidelity Aerostructural Optimization of a Transport Aircraft Configuration,” *Journal of Aircraft*, Vol. 51, 2014, pp. 144–160. doi:[10.2514/1.C032150](https://doi.org/10.2514/1.C032150).
- [32] Liem, R. P., Kenway, G. K. W., and Martins, J. R. R. A., “Multimission Aircraft Fuel Burn Minimization via Multipoint Aerostructural Optimization,” *AIAA Journal*, Vol. 53, 2015, pp. 104–122. doi:[10.2514/1.J052940](https://doi.org/10.2514/1.J052940).
- [33] Gray, J. S., Hearn, T. A., Moore, K. T., Hwang, J. T., Martins, J. R. R. A., and Ning, A., “Automatic Evaluation of Multidisciplinary Derivatives Using a Graph-Based Problem Formulation in OpenMDAO,” *15th AIAA/ISSMO Multidisciplinary Analysis and Optimization Conference*, American Institute of Aeronautics and Astronautics, August 2014. doi:[10.2514/6.2014-2042](https://doi.org/10.2514/6.2014-2042).
- [34] Hearn, D. T., Hendricks, E., Chin, J., Gray, J., and Moore, D. K. T., “Optimization of Turbine Engine Cycle Analysis with Analytic Derivatives,” *17th AIAA/ISSMO Multidisciplinary Analysis and Optimization Conference, part of AIAA Aviation 2016 (Washington, DC)*, 2016. doi:[10.2514/6.2016-4297](https://doi.org/10.2514/6.2016-4297).
- [35] Gray, J., Chin, J., Hearn, T., Hendricks, E., Lavelle, T., and Martins, J. R. R. A., “Thermodynamics For Gas Turbine Cycles With Analytic Derivatives in OpenMDAO,” *57th AIAA/ASCE/AHS/ASC Structures, Structural Dynamics, and Materials Conference, AIAA SciTech*. doi:[10.2514/6.2016-0669](https://doi.org/10.2514/6.2016-0669).
- [36] Kenway, G. K., Kennedy, G. J., and Martins, J. R. R. A., “A CAD-Free Approach to High-Fidelity Aerostructural Optimization,” *Proceedings of the 13th AIAA/ISSMO Multidisciplinary Analysis Optimization Conference*, No. AIAA 2010-9231, Fort Worth, TX, Sept. 2010. doi:[10.2514/6.2010-9231](https://doi.org/10.2514/6.2010-9231).
- [37] Heath, C. M., Slater, J. W., and Rallabhandi, S. K., “Inlet Trade Study for a Low-Boom Aircraft Demonstrator,” *Journal of Aircraft*, 2016. doi:[DOI: 10.2514/1.C034036](https://doi.org/10.2514/1.C034036).
- [38] Lambe, A. B. and Martins, J. R. R. A., “Extensions to the Design Structure Matrix for the Description of Multidisciplinary Design, Analysis, and Optimization Processes,” *Structural and Multidisciplinary Optimization*, Vol. 46, 2012, pp. 273–284. doi:[10.1007/s00158-012-0763-y](https://doi.org/10.1007/s00158-012-0763-y).